Electroactive Oligoaniline-Containing Self-Assembled Monolayers for Tissue Engineering Applications[†]

Yi Guo,[‡] Mengyan Li,[§] Andreas Mylonakis,[‡] Jingjia Han,[§] Alan G. MacDiarmid,[⊥]
Xuesi Chen,[#] Peter I. Lelkes,*[,§] and Yen Wei*[,‡]

Department of Chemistry and School of Biomedical Engineering, Science and Health Systems, Drexel University, Philadelphia, Pennsylvania 19104, Department of Chemistry, University of Pennsylvania, Pennsylvania 19104, and Changchun Institute of Applied Chemistry, Chinese Academy of Science, People's Republic of China 130022

A novel electroactive silsesquioxane precursor, *N*-(4-aminophenyl)-*N*′-(4′-(3-triethoxysilyl-propyl-ureido) phenyl-1,4-quinonenediimine) (ATQD), was successfully synthesized from the emeraldine form of amino-capped aniline trimers via a one-step coupling reaction and subsequent purification by column chromatography. The physicochemical properties of ATQD were characterized using mass spectrometry as well as by nuclear magnetic resonance and UV−vis spectroscopy. Analysis by cyclic voltammetry confirmed that the intrinsic electroactivity of ATQD was maintained upon protonic acid doping, exhibiting two distinct reversible oxidative states, similar to polyaniline. The aromatic amine terminals of self-assembled monolayers (SAMs) of ATQD on glass substrates were covalently modified with an adhesive oligopeptide, cyclic Arg-Gly-Asp (RGD) (ATQD−RGD). The mean height of the monolayer coating on the surfaces was ∼3 nm, as measured by atomic force microscopy. The biocompatibility of the novel electroactive substrates was evaluated using PC12 pheochromocytoma cells, an established cell line of neural origin. The bioactive, derivatized electroactive scaffold material, ATQD−RGD, supported PC12 cell adhesion and proliferation, similar to control tissue-culture-treated polystyrene surfaces. Importantly, electroactive surfaces stimulated spontaneous neuritogenesis in PC12 cells, in the absence of neurotrophic growth factors, such as nerve growth factor (NGF). As expected, NGF significantly enhanced neurite extension on both control and electroactive surfaces. Taken together, our results suggest that the newly electroactive SAMs grafted with bioactive peptides, such as RGD, could be promising biomaterials for tissue engineering.

1. Introduction

Polymeric scaffold materials employed in tissue engineering have been intensely studied because they are crucial to restoring or replacing biological functions.[1] In order to be useful as provisional extracellular matrix (ECM) substitutes, the scaffolds have to be biomimetic, in addition to being biocompatible, absorbable, and biodegradable and exhibiting tissue-specific mechanical properties. In the past, numerous synthetic polymers, natural biopolymers, or composite copolymers, such as, respectively, poly(ε-caprolactone), polylactide, lyophilized elastin−collagen, and chitosan (CS)-based biocomposites, have been used for tissue engineering applications.[2] More recently, novel biomaterials have emerged, which, through targeted function-alization, are tailored to trigger specific cell growth and differentiation.[3]

One particularly exciting area of tissue engineering is the repair of spinal cord injuries. In many of these studies, novel permissive scaffolds are evaluated, with the aim that these scaffolds will aid in the migration and maintenance/differentiation of endogenous (or exogenously seeded) neurons and facilitate the establishment of functional axonal bridges across the site of lesion in the spinal cord. PC12 pheochromocytoma cells are cloned cells derived from the neural crest, which, in the presence of neurotrophic factors, such as nerve growth factor (NGF), can differentiate into a neuronal phenotype.[4] Because of the ease of their availability, PC12 cells are well established as a model system to study neuronal differentiation.[5]

Since the 1970s, electrically conductive organic polymers, such as polypyrrole (PPy) and polyaniline (PANi), have been extensively explored for many new technologies.[6] For instance, PANi was used to fabricate high-performance biosensors upon surface modification of electrodes.[7] In recent years, this unique class of "synthetic metals" has gained growing interest in a variety of biomedical applications, which exploit the intrinsic physicochemical properties of conducting polymers to interact with the biological environment.[8] Recent reports described the use of conducting polymers as electroactive scaffold or substrate materials in tissue engineering to support and modulate the growth and differentiation of electrically excitable cells, such as PC12 pheochromocytoma cells[9] or bone marrow stromal cells.[10] The motivation for culturing cells and tissues on electroactive surfaces is based on the assumption that an

* Corresponding author. (1) Yen Wei, Ph.D., Herman B. Wagner Professor of Chemistry, Director of The Center for Advanced Polymers and Materials Chemistry, Department of Chemistry, Drexel University, Philadelphia, Pennsylvania 19104, USA. Tel. (O) (215) 895-2650; (Lab) -1644, -2979, and -2982. Fax (215) 895-1265. E-mail: weiyen@drexel.edu. (2) Peter I. Lelkes, Ph.D., Calhoun Chair Professor, School of Biomedical Engineering & Engineering, Drexel University, Philadelphia, PA 19104, USA. Tel. (O) (215) 762-2071; (Lab) -7234. Fax (215) 895-4983. E-mail: pilelkes@drexel.edu.

[†] Professor Alan MacDiarmid, the 2000 Nobel Prize Laureate for his discovery of conductive polymers, and a keen participant in this research, died on February 7, 2007 after a long, courageous battle with cancer. It is with great pride and sadness that we dedicate this paper to his memory.

[‡] Department of Chemistry.

[§] School of Biomedical Engineering, Science and Health Systems, Drexel University.

[⊥] University of Pennsylvania.

[#] Chinese Academy of Science.

Scheme 1. Synthetic Scheme of ATQD (B) as well as EBAT (A) and TSUPQD (C)
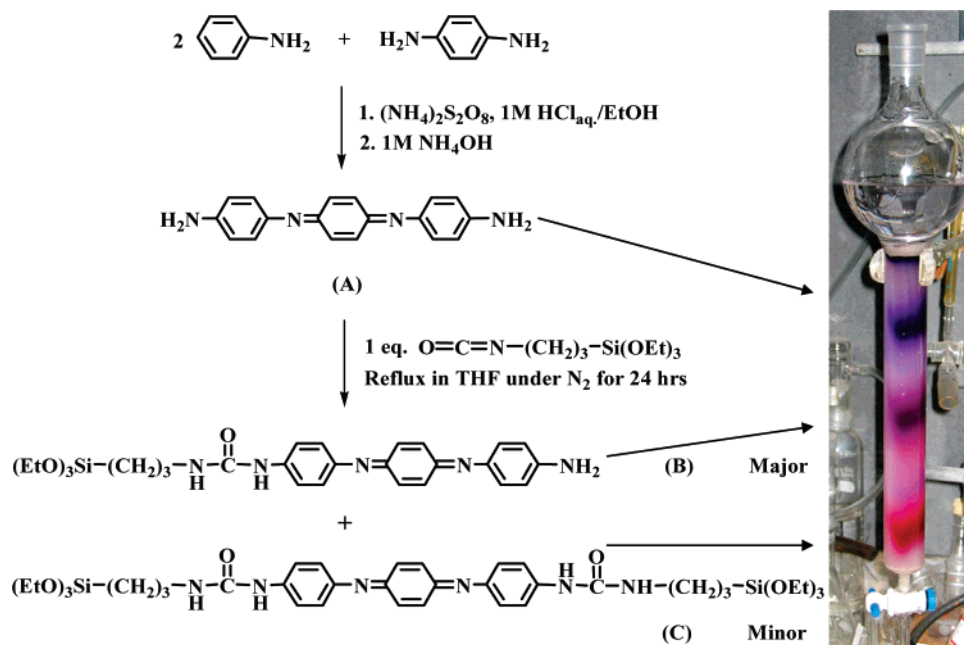
electrical stimulus could tune the morphology and function of the anchorage-dependent cells through the specific interaction.[11] While the mechanism of how external electrical currents may contribute to cellular activation is not fully understood, it is well documented that electrical stimulation plays an important role in enhancing the neurogenic[12] and osteogenic[13] commitment of cells when grown on electroactive scaffolds derived from PPy.[14] Schmidt and co-workers have demonstrated that electrical stimulation enhances NGF-induced neuritogenesis in PC12 cells grown on PPy.[12] Similarly, Shastri et al. reported the electrical stimulation-enhanced osteogenic differentiation of bone marrow stromal cells cultured on PPy.[13] More recently, several other electroactive scaffolds composed of PPy-based biocomposites have been developed for studying cell growth in vitro and cytotoxicity in vivo.[15]

In contrast, few studies have reported the potential tissue engineering applications of PANi, which is one of best characterized conducting polymers, with its diversity of structural forms, high environmental stability, and ease of charge transport by the so-called "doping/dedoping" process.[16] The main challenge in using PANi for biotechnological applications arises from its apparently poor cell compatibility.[17] Covalent grafting of bioactive molecules, such as adhesion peptides, is one effective strategy to improve the biocompatibility of conventionally non-biocompatible materials. We previously reported that PANi films functionalized with the bioactive laminin-derived adhesion peptide YIGSR (Tyr-Ile-Gly-Ser-Arg) exhibited significant enhanced PC12 cell attachment and differentiation.[18] In studying the influence of the surface conductivity of the emeraldine salt form of PANi on H9c2 rat cardiac myoblast cells, we determined that, for these cells, adhesion to and proliferation on unmodified electrical conductive PANi surfaces was essentially the same as that on tissue-culture-treated polystyrene (TCP).[19] More recently we demonstrated the biocompatibility of electrospun nanofibers containing camphorsulfonic acid-doped PANi and gelatin, which might serve as potential scaffold materials for cardiac tissue engineering.[20] The utilization of PANi-based materials, however, is still restricted by the processability, biodegradability, and resorbability of the conductive polymer.

To the best of our knowledge, no reports have been published that focus on the biocompatibility of novel substrate materials containing electroactive oligoanilines. In particular, the amino-capped emeraldine base form of aniline trimer (EBAT) might serve as a promising candidate because of its well-defined electroactive structure, high flexibility during synthesis and processing, and ease of degradability.[21] In this paper, we describe a novel electroactive silsesquioxane precursor, *N*-(4-aminophenyl)-*N*′-(4′-(3-triethoxysilylpropyl-ureido) phenyl-1,4-quinonenediimine) (ATQD), which was synthesized via a one-step coupling reaction between EBAT and triethoxysilylpropyl isocyanante (TESPIC). Our data indicate that ATQD could be evenly coated onto the glass surface via condensation and self-assembly. Furthermore, an Arg-Gly-Asp (RGD)-sequence-containing oligopeptide, cyclo(Arg-Gly-Asp-D-Phe-Lys) [cyclo-(RGD-D-FK)], was covalently grafted onto the free aromatic amino-end of ATQD to improve its biocompatibility, as assessed by the adhesion, proliferation, and differentiation of rat PC12 pheochromocytoma cells.

2. Experimental Section

2.1. Materials. TESPIC, anhydrous tetrahydrofuran (THF), dimethylformamide (DMF), and *n*-hexane were purchased from Aldrich (Milwaukee, WI), and were used without further purification. *N*-hydroxysuccinimidobiotin (NHS-biotin), ImmunoPure avidin, and 2-(4′-hydroxyazobenzene) benzoic acid (HABA) were purchased from PIERCE (Rockford, IL). The cyclic RGD peptide cyclo(RGD-D-FK) was supplied by Peptides International (Cat. No. PCI-3661-PI, Louisville, KY). *N,N*′-bis(4′-aminophenyl)-1,4 quinonenediimine (EBAT) was prepared according to a method developed in our group and purified with acetone in a Soxhlet extractor.[22] All cell culture media and supplements were from Hyclone (Logan, UT), and disposable tissue culture supplies were from Fisher (Corning, NY).

2.2. Synthesis, Purification, and Characterization of ATQD. As described in Scheme 1, equal molar amounts of purified EBAT and TESPIC were mixed in a three-neck round flask containing anhydrous THF with magnetic stirring prior to refluxing at ~67 °C for 24 h under N_2 atmosphere. After being cooled to room temperature, nonpolar solvent *n*-hexane was quickly added to the newly formed, red-wine-colored solution, and the reaction system was immediately moved into

a dry-ice−acetone bath for another 12 h to allow thorough precipitation. The dark violet solid was collected by vacuum filtration through filter paper (No. 42, 11.0 cm, Whatman), washed with 300 mL of n-hexane, and dried under vacuum for 3 days at room temperature, resulting in a yield of ∼85%. Further purification was achieved by silica gel column chromatography using n-hexane/ethanol (3/1, v/v) as eluant (thin layer chromatography (TLC), $R_f = 0.8$), followed by solvent evaporation in a rotary evaporator (RE111 Rotavapor, Brinkman). The resulting product was subsequently characterized by ^{1}H NMR and ^{13}C NMR performed on a Varian 300 MHz NMR spectrometer; UV−vis spectra were acquired on a Perkin-Elmer Lambda 35 UV−vis spectrometer, and mass spectra (MS) were obtained on a VG70SE using fast atom bombardment (FAB) with 30 kV Cs ion bombardment. Electrochemical measurements were performed using an Epsilon Potentiostat interfaced to a PC computer. A three-electrode system was employed, consisting of a platinum working disk electrode (surface area (s) = 0.02 cm^2), a platinum-wire auxiliary electrode, and a reference electrode. The reference electrode was Ag/Ag$^+$ (silver ions as AgNO$_3$ (0.01 M) in a solution of MeCN containing 0.1 M Et$_4$NBF$_4$). The scan rate used was 60 mV/sec.

2.3. Fabrication and Characterization of ATQD−RGD Self-Assembled Monolayers (SAMs). Prior to chemical modification, 15 mm diameter circular glass coverslips (Fisher) were precleaned following the Radio Corporation of America (RCA) cleaning process[23] to generate a fresh, thin silica layer, the surface of which was rich in Si−OH groups. Briefly, the glass substrates were placed in a 5:1:1 (v) H$_2$O/H$_2$O$_2$/NH$_4$OH solution to remove insoluble organic contaminants, then submerged in a solution of H$_2$O/HF (v/v ∼ 100:1) to remove possible thin SiO$_2$ layers, followed by ionic cleaning using a solution of 6:1:1 (v) H$_2$O/H$_2$O$_2$/HCl. Freshly prepared coverslips were dried in N$_2$ atmosphere and then immediately immersed in an acetone solution of ATQD at room temperature. The slides were left in that solution for 24 h in order to allow the ATQD chains to attach to the wafer surface and to form SAMs. Subsequently, the slides were thoroughly washed by with acetone and 0.1 N HCl. The progress of surface modification was monitored by atomic force microscopy (AFM) and quantified using a biotinylation-based procedure. In brief, at various time points (0−24 h), individual samples were transferred into a Nanoscope IIIa AFM (Digital Instruments/Veeco, Santa Barbara, CA) equipped with rectangular silicon nitride cantilevers (TESPW, Digital Instruments/Veeco) using the tapping mode for the height visualization of ATQD on the glass surface. The degree of surface modification/ functionalization with ATQD was evaluated quantitatively by examining the amount of the free aromatic amine groups using a biotin-labeling method, which has been commonly used in nonradioactive labeling and detection.[24] The azo-dye HABA absorbs light at 500 nm when it binds to avidin. Because of its stronger affinity for avidin, the biotin moieties in biotinylated ATQD samples can replace HABA from its interaction with avidin. Therefore, immersion of biotinylated ATQD substrates into the HABA−avidin solution results in a blue shift of the absorbance peak to 356 nm and a corresponding decrease of the absorbance at 500 nm. The change in absorbance can proportionally reflect the number of available biotin groups attached to the surface. The calculations are based on Beer's law: $A_\lambda = \epsilon_\lambda bC$, where ϵ is extinction coefficient (34 000 mL/(M^{-1} cm^{-1})) at wavelength λ (500 nm), b is the cell path length (1 cm), and C is the concentration of the sample (mmol/mL). For each sample in this study, amine groups of ATQD were biotinylated with an NHS-biotin solution (10 mg dissolved in 3 mL of DMF)[25] to obtain biotin-labeled substrates. The progress of biotinylation of the derivatized substrates was evaluated by placing them into a HABA/avidin solution (7.2 µg HABA + 0.5 mg avidin/mL in pH 7.2 phosphate-buffered saline (PBS)) and measuring the change in absorbance of the chromophore at 500 nm (A_{500}). The density of the free amine group was expressed as the concentration of biotin in millimoles per milliliter according to the formula $D_{NH2} = \Delta A_{500}/$ (34 000b), where b is path length (1 cm).

The ATQD-modified substrates were cross-linked with glutaraldehyde (2.5%, adjusted to pH 7 using 0.1 N NaOH) for 1 h at ∼30 °C, followed by extensive rinsing in deionized water to remove excess glutaraldehyde. Next, the activated, cross-linked surfaces were exposed (37 °C, 1 h) to acetic acid/acetate buffer (pH 5) containing a cyclic RGD peptide (5 µg/mL). After immobilization of the bioactive molecules, the substrates were cleaned by rinsing with distilled water and PBS and then used immediately for cell culture to avoid any contamination.

2.4. Cell Culture. To validate the suitability of electroactive oligoanilines as scaffold materials for tissue engineering, we used rat neuronal pheochromocytoma PC12 cells. These cells were maintained in a humidified incubator and grown in Dulbecco's modified Eagle's medium (DMEM) supplemented with 7.5% horse serum (Hyclone), 7.5% fetal bovine serum (Hyclone), 1% L-glutamine, an antibiotic cocktail (50 mg/mL penicillin and 100 IU/mL streptomycin) under standard conditions (37 °C, 5% CO$_2$). For the in vitro biocompatibility studies, PC12 cells were seeded at various densities (depending on the experimental protocol) onto circular glass cover slips, which were either untreated (controls) or coated with the novel substrates and placed inside 24-well tissue culture plates. Before seeding, all cover slips were sterilized by exposure to UV radiation for 1 h at both sides and secured to the bottom of wells by Viton O-rings (Cole-Parmer).[26]

For the attachment studies, PC12 cells were seeded in 1 mL of complete DMEM at a density of 50 000 cells/well in 24-well tissue culture plates. At various time points (1−24 h), the number of attached cells on the substrates and unattached cells in the supernatants was assessed by manual counting in a hemocytometer (Fisher). The degree of cell adhesion was determined by dividing the number of attached cells by the total number of cells seeded. In addition, cell attachment to the substrates was also assayed biochemically, using the Alamar Blue (AB) assay (Biosource, Alameda, CA).[27,28]

Cell proliferation was also evaluated continually with the AB assay for a 13-day culture period, as previously described.[29] Since we used all the substrates to culture the cells with the serum-containing medium, we compared the differences of all the substrates on cells under the same medium conditions. For the proliferation studies, cell seeding density was optimized at 50 000 PC12 cells/well on the basis of the preliminary results. The alamar fluorescence data in the proliferation study were normalized to the initial fluorescence readings at day 1. The cell growth rate K' for the exponential phase (days 3−9) was calculated using the following equation: $K' = [\ln(N_2/N_1)]/(T_2 - T_1)$, where N_1 and N_2 are the normalized cell numbers at time 1 (T_1) and time 2 (T_2), respectively; the population doubling time (PD) was determined as PD = (ln 2)/K'.[30]

In order to evaluate the influence of the electroactive substrates on the neuronal differentiation of PC12 cells, neurite growth was assessed using microscopic techniques. PC12 cells were seeded on the various substrates at a density of 10 000 cells/well and were allowed to differentiate in the absence and presence of NGF (50 ng/mL). The cultures were photographed on days 1, 3, 6, and 10. Before imaging, samples were fixed with 10% buffered formalin for 15 min at room temperature, stained with 2 µg/mL bisbenzimide (Hoechst 33258, a nuclear stain, Sigma) and 1 µg/mL rhodamine−phalloidin (F-actin stain, Sigma, P1951) in PBS solution containing 0.2% Triton-X 100 (Sigma) for 10 min, and washed carefully with PBS three times for 5 min each. Digital fluorescence and phase contrast images of the cells were acquired using a Leica DMRX microscope equipped with appropriate optics and filters using a Leica 300F camera. Spontaneous and NGF (50 ng/mL, Sigma, N2513)-induced neurite outgrowth was analyzed from phase contrast images (>20 per sample) of cells growing on ATQD−RGD and TCP substrates at the designated time points. The public-domain imaging software "Image J" was used to measure the neurite length of PC12 cells in our pictures, assessing the length of the neurites from the cell body to the furthest tip of the extension.

2.5. Statistics. The number of independent replicates used for statistical analysis is listed individually for each experiment. Where

Scheme 2. Schematic Representation of Fabricating ATQD−RGD SAMs
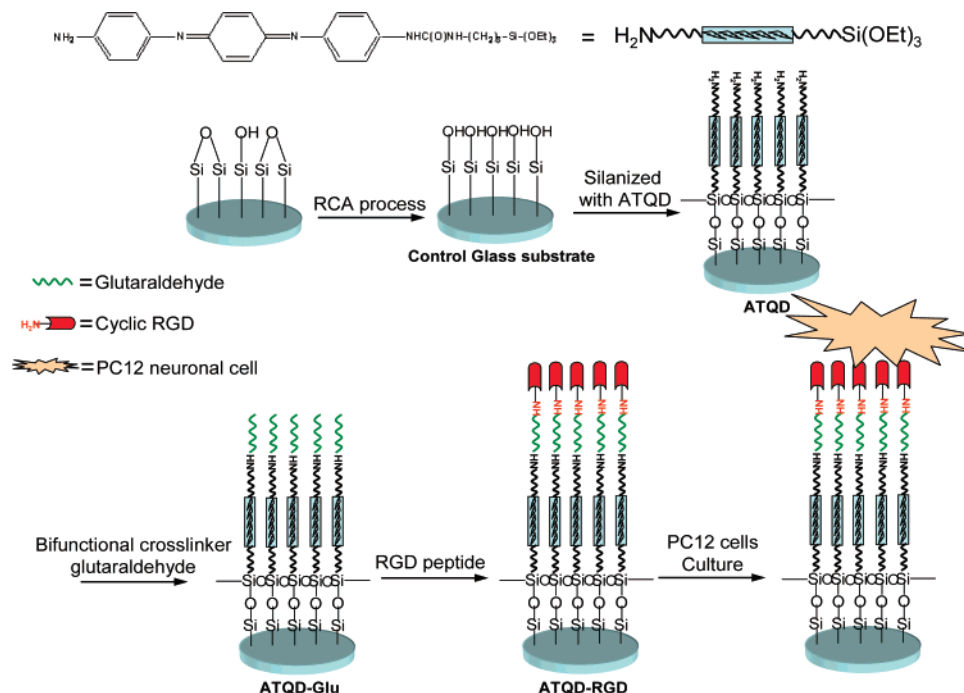
appropriate, the data are presented as mean ± standard deviation (SD). Student's t-test was used to analyze the statistical variability of the data, with $p < 0.05$ being statistically significant.

3. Results and Discussion

3.1. Physicochemical Properties of the Novel Electroactive Silsesquioxane Precursor, ATQD. In this paper we describe, for the first time, the synthesis of an oligomeric analogue of conducting PANi, the novel electroactive ATQD. We hypothesize that this novel compound might possess several properties, which, in comparison to its macromolecular counterparts, might render ATQD advantageous for tissue engineering applications (see Scheme 2).

• ATQD contains useful heterobifunctional end groups, one for anchoring onto (negatively) charged substrates (in this case, glass) and the other one available for covalent grafting of (positively charged) biomolecules, such as amino acids or phospholipids. Hence, ATQD can be considered a new electroactive model compound for other aniline oligomers providing a wide range of potential biomedical applications as scaffold materials.

• Rather than forming horizontal film surfaces, the self-assembly of the electroactive oligomeric aniline chains is stabilized by intermolecular hydrogen bonding, resulting in an orientation perpendicular to the surfaces and, hence, facilitation of cell attachment to the functionalized three-dimensional substrate.

• Aniline oligomers can be tailored to exhibit improved processability and biodegradability[31] while maintaining a well-defined structure and electroactivity during the biomodification.

• Since bioactive peptide motifs, such as cyclic RGD, are grafted as a final step onto SAMs, seeded cells will be in direct contact with bioactive peptide sequences on the outer surface. Unlike linear peptides, cyclic RGD exhibits greater structural stability and higher flexibility in functionalization via the lysine residues,[32] resulting in improved biocompatibility.
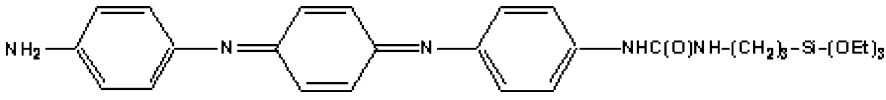
As described in the synthesis pathway (Scheme 1), the solid product obtained via the one-step isocyanatoamine coupling reaction between equivalent moles of EBAT and TESPIC yielded the desired compound, ATQD, as well as the byproduct,

N,N'-bis(4'-(3-triethoxysilylpropyl-ureido)phenyl)-1,4-quinonenenediimine (TSUPQD). Hence, it was essential to purify ATQD from the crude product, prior to any further characterization and processing/functionalization. When using silica gel column chromatography, the second, dark-pink fraction was identified as pure ATQD, which is actually the "intermediate" product between TSUPQD and EBAT; this result is consistent with the preliminary examination of the crude product by TLC (see Supporting Information, Figure S1).

The molecular structure of ATQD was characterized by ^{1}H and ^{13}C NMR spectroscopy (Figures S2 and S3, Supporting Information) in DMSO-d_6, with tetramethylsilane as the internal standard, and mass spectrometry. The NMR peak assignments are listed in Table 1. The impurity peaks observed in both of the NMR spectra can be attributed to the residual solvents n-hexane and ethanol. In addition, the MS of ATQD were recorded using FAB ionization (Figure S4 and Table S1, Supporting Information). In the low-resolution mode, the peak at 537.07 *m/z* represents the ATQD emeraldine salt form (M + 2H[+]), while, in high-resolution mode, the exact mass was determined to be 537.2752, on the basis of the mass calibration standard compound polypropylene glycol. The calculated mass and the as-deduced elemental composition of ATQD are in good agreement with the expected ATQD molecular formula, $C_{28}H_{39}N_5O_4Si$.

The optical absorption spectra (Figure 1) of ATQD, EBAT, and TSUPQD in ethanol show a typical broad quinoid (Q) absorption peak centered at ca. 520−590 nm and a narrower benzenoid (B) peak centered at ca. 330−340 nm. Both of these peaks are routinely observed for the emeraldine base form of PANi derivatives. Similar to that for PANi, the Q peak is associated with the excitonic transition of $\pi_b-\pi_q$ from the benzene unit to the quinone unit, while the B peak results from a $\pi-\pi^*$ transition in the benzene unit.[33] The Q peak exhibits a noticeable blue shift, while the Q/B intensity ratio decreases with the degree of modification from EBAT (Figure 1, curves b and c), suggesting that the enhanced conjugation arising from covalent modification by ureido groups leads to stronger electronic resonance. Therefore, the peak position (Q = 550

**Table 1.** ^{1}H NMR and ^{13}C NMR Spectra Explanations

$^{1}H-$NMR	$\delta = $ **8.35** (singlet for one H in $-(C{=}O)-NH-$ close to aromatic ring); $\delta = $ **7.70**, **7.45**, **7.20**, and **6.88** (multiplet for 12 allyl H from aniline trimer); $\delta = $ **6.10** (triplet for another urea H); $\delta = $ **5.40** (singlet for two aromatic amines); $\delta = $ **3.80** (multiplet for six ethylene H in $-SiOCH_2CH_3-$); $\delta = $ **3.05** (multiplet for two ethylene H close to the amine group in $-CH_2CH_2NH-$); $\delta = $ **1.48** (multiplet for two middle ethylene H in $-CH_2CH_2CH_2-$); $\delta = $ **1.25** (triplet for nine methyl H in $-SiOCH_2CH_3-$); $\delta = $ **0.56** (multiplet for two ethylene H close to silica in $-CH_2CH_2CH_2Si-$).
$^{13}C-$NMR	$\delta = $ **66.2**, **31.0** ($-SiOCH_2CH_3-$); $\delta = $ **41.2**, **24.0**, **8.1** ($-CH_2CH_2CH_2-$). $\delta = $ **164.5** (C=O); $\delta = $ **154.8**, **154.0**, **149.0**, **148.2**, **147.0**, **146.2**, **139.2**, **138.4**, **129.5**, **128.8**, **119.2**, **118.0** (aryl C).
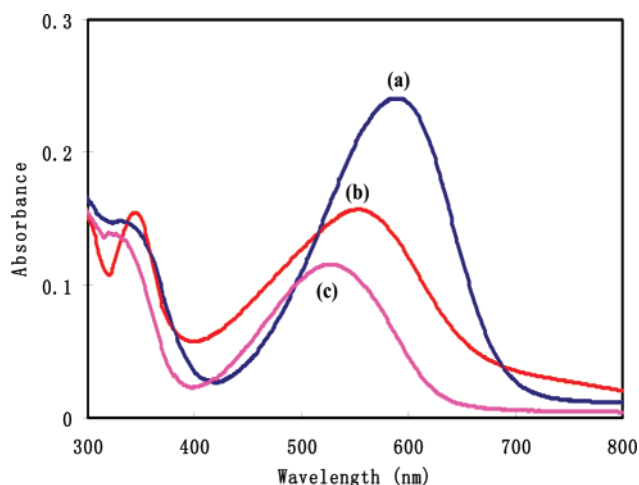
Figure 1. UV−vis spectrum of (a) EBAT, (b) ATQD, and (c) TSUPQD. Solvent: ethanol (EtOH). All three compounds were purified before characterization and measured under the same concentration.

Figure 2. Cyclic voltammogram of ATQD in acetonitrile containing 0.1 M Et_4NBF_4 and 0.5 M $MeHSO_4$. The scan rate used was 60 mV/s.

nm) and relative band intensity (Q/B = 1.05) of monofunctionalized ATQD (Figure 1, curve b) are intermediate with regard to those values for TSUPQD and EBAT.

The cyclic voltammogram of ATQD, recorded in a nonaqueous solution of MeCN containing 0.1 M Et_4NBF_4 and 0.05 M $MeHSO_4$ (Figure 2), is, as expected, essentially similar to the voltammogram of the acid-doped form of PANi.[34] The first two pairs of the well-defined redox peaks at 320 and 440 mV respectively represent the removal/addition of one electron each, and can be attributed to the reversible redox process from the "leucoemeraldine" to the ''emeraldine'' form (Figure 2a). Moving progressively to higher potentials, two reversible redox peaks with formal potentials of 650 and 740 mV, respectively, can be observed, each of which represents the removal/addition of one electron. These are assigned to the oxidation/reduction of the "emeraldine" form to the "pernigraniline" form and correspond to the nonsubstituted end of the ATQD (Figure 2b). At even higher potentials (∼950 mV), another pair of peaks is observed representing the oxidation/reduction of the "emeraldine" to the "pernigraniline" form, but corresponding to the substituted end of the aniline trimer moiety (Figure 2c). These well-defined redox peaks represent the removal/addition of two electrons. The electron-withdrawing ureido group of ATQD causes the redox peaks of the substituted end group to be shifted anodically and makes them discernible from the redox peaks of the nonsubstituted end group.

3.2. Surface Characterization of Novel Electroactive ATQD−RGD SAMs. Our strategy (Scheme 2) employs the immobilization of bioactive peptides onto the electroactive substrates in order to render them biocompatible. Some of these
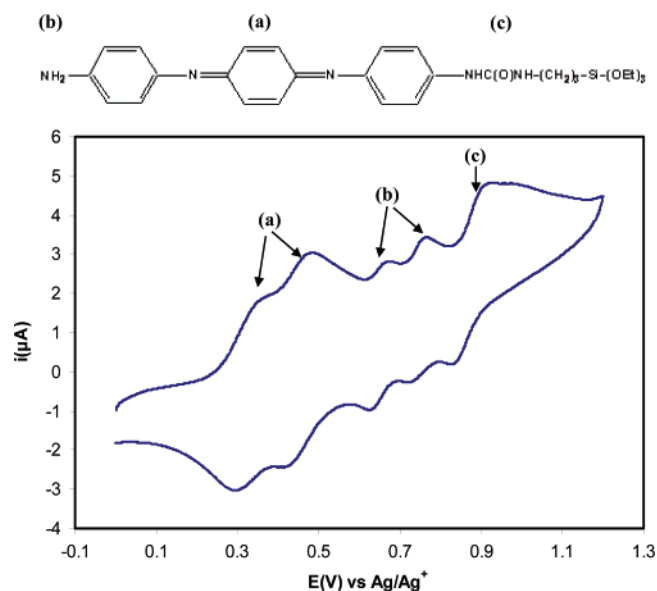
peptides can serve as cell surface receptor-recognizable sequences (RGDs). The chemical functionalization of the surface was technically achieved via the self-assembly of our novel organosilane, ATQD, on the silanolized surface, which occurred as a result of the hydrolysis of ethylortho groups and the condensation reactions that lead, in turn, to the formation of a strong Si−O−Si bond. A chemical cross-linker, glutaraldehyde,[35] was then utilized, which, at one end, is covalently bound to the prosthesis surface and, at the other end, is bound to the bioactive molecules. As detailed in the experimental section, the RCA process can effectively activate the glass surface, generating silanol groups while removing potential hydrophobic contaminants. This curing process has to be fine-tuned on a case-by-case basis in order to obtain optimal SAMs.

Shown in Figure 3 are typical AFM images, which reveal the correlation between exposition to the ATQD solution and the resulting SAMs on the glass surface. As the freshly washed silicon surface appears ultraflat (Figure 3a), the morphology of SAMs after ATQD treatment is easily distinguishable from that of the background. As seen in Figure 3b−d, the thickness and complexity of the ATQD layer increased with increasing exposure time, until, after 24 h of exposure, a densely packed layer was formed. The ATQD surface coverage is quite uniform in the height and amplitude. An AFM height profile for 24 h modification (Figure 3e) exhibited a mean height of 3.0 nm. Nevertheless, as seen in Figure 3d, a few larger chains can also be found on the edge of the scanning region (2 × 2 μm). A
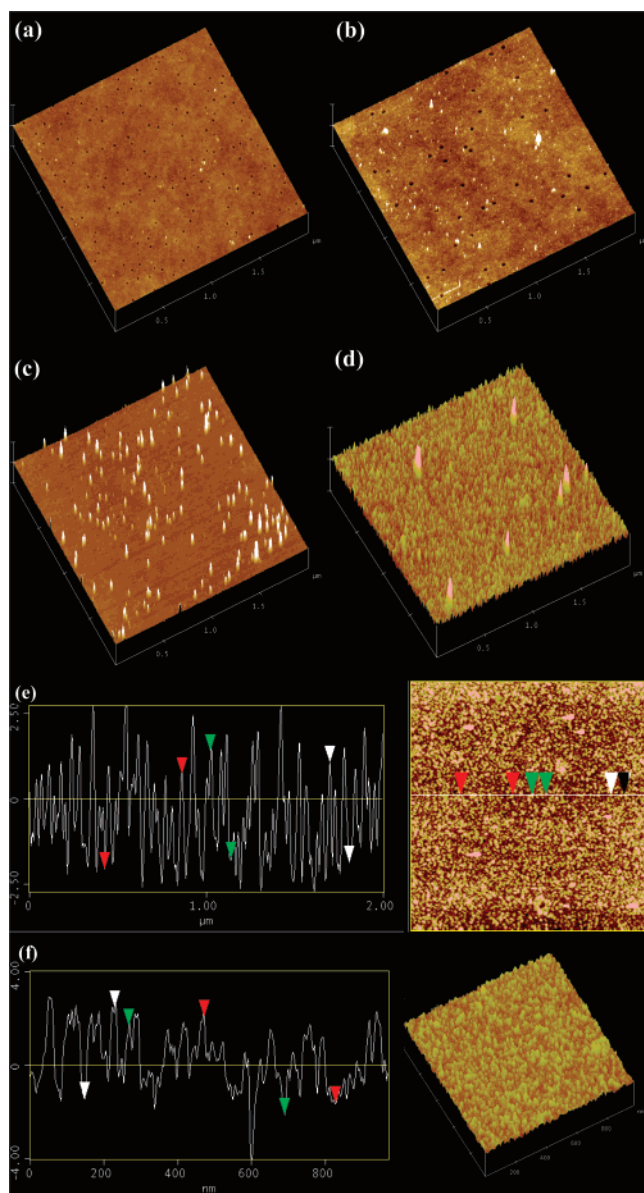
Figure 3. AFM tapping-mode images of the ATQD SAMs at various time courses: (a) 0 h; (b) 1 h; (c) 6 h; (d) 24 h. Panels a–d are height images of a 2 μm scan. Panel e shows a height profile and a top-view image of ATQD–SAMs at 24 h. Panel f shows a height profile and height image of a 1 μm scan for ATQD–RGD SAMs.

plausible explanation is that these spots might reflect a few residual defects or organic contaminants on the glass surface. Upon the binding of cyclic RGD, the average height is slightly increased to 3.8 nm, indicating the presence of the "umbrellas" on the outer surface (Figure 3f).

The degree of surface modification/functionalization with ATQD was evaluated quantitatively by examining the amount of the free aromatic amine groups using a biotin-labeling method, described in detail in the Materials and Methods section. As seen from the kinetics of surface modification (Figure 4), the content of ATQD increases sharply after 6 h (14.9 ± 0.21 10^{-7}mmol/sample; $n = 3$) and gradually reaches saturation within 24 h (25.5 ± 0.31 10^{-7}mmol/sample; $n = 3$). Although more ATQD might still be covalently bound to the surface with longer treatment, the homogeneous SAMs formed within 24 h should suffice for the subsequent peptide binding of peptide and biocompatibility studies.

3.3. Cell Adhesion. In order to validate the usefulness of ATQD for tissue engineering applications, we first tested its
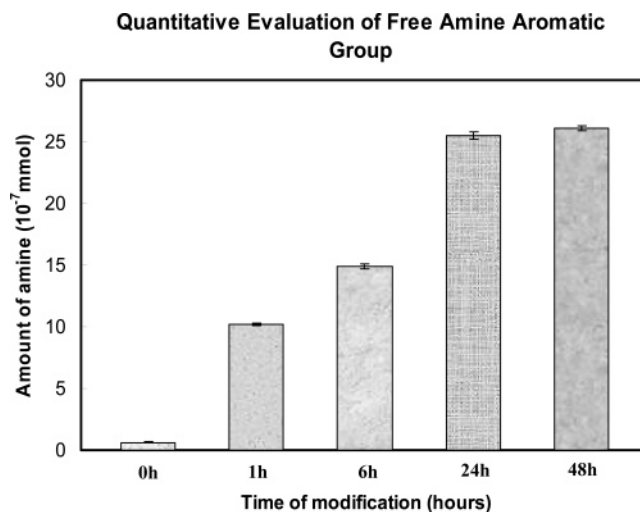

Figure 4. Quantization evaluation of ATQD SAMs via a biotin-labeling method at various time points.
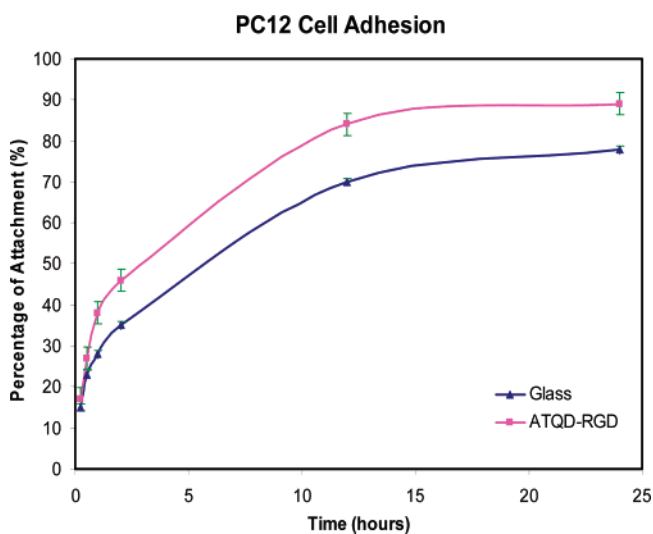

Figure 5. Cell attachment study. Attachment comparison between glass control and ATQD–RGD via manual counting. Data are expressed as means $\pm$ SD, $n = 3$.

biocompatibility to ascertain that, at the minimum, this novel material will promote cell adhesion/proliferation and function in vitro.

To determine PC12 cell adhesion to ATQD-modified surfaces, the number of adhered cells was determined both by manual cell counts and use of the AB assay. Shown in Figure 5 is the kinetics of cell attachment, represented as the average percentage of attached cells to the total number of seeded cells. About 45% of the seeded cells were attached to RGD–ATQD substrates within 2 h. By 12 h, approximately 85% of the seeded cells were attached; attachment plateaued thereafter, reaching a maximum of 90% after 24 h.

Importantly, the percentage of PC12 cells attached after 2 h to the RGD–ATQD surface ($46 \pm 2.1\%$; $n = 3$) was always significantly ($p < 0.01$) higher than that attached to the control nonderivatized ATQD surface ($34 \pm 1.7\%$; $n = 3$), suggesting that the attachment of PC12 cells can be significantly improved by the covalently conjugated RGD moiety.

Our initial results on cell adhesion were further validated using a biochemical (AB) assay (see Figure S5, Supporting Information). The kinetics of cell attachment obtained in the AB assay is in reasonable agreement with that obtained from manual counting, indicating that 12 h could be deemed as the
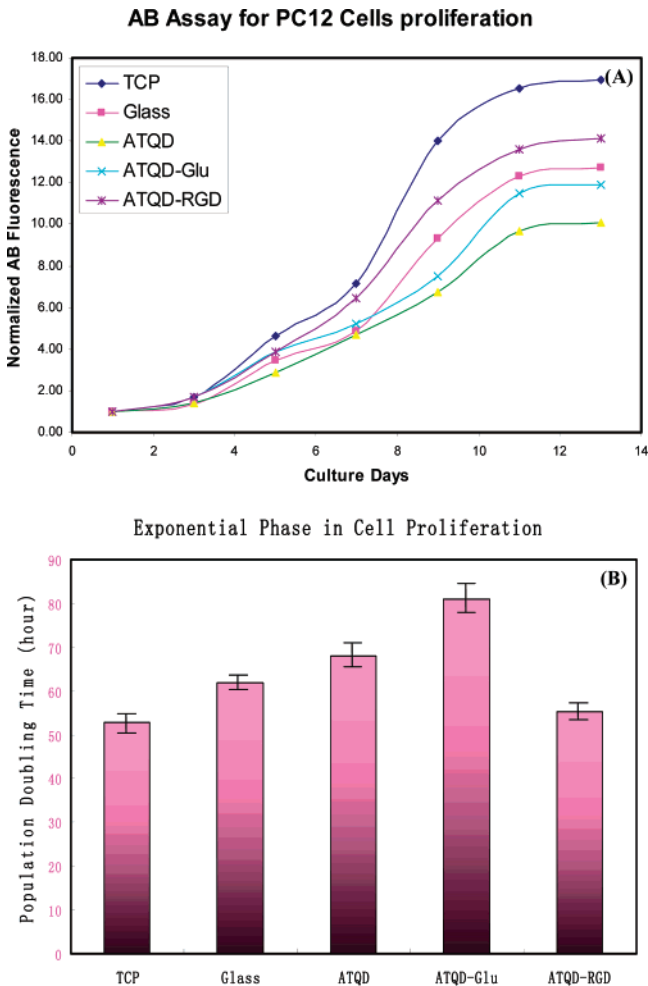
Figure 6. PC12 cell proliferation on various substrates over a 13 day time course. (A) Cell proliferation/metabolic activity were evaluated using the AB Assay. (B) Chart of population doubling time over the exponential phase. The data were normalized to the AB fluorescence reading at day 1. Data are expressed as means $\pm$ SD, $n = 3$.
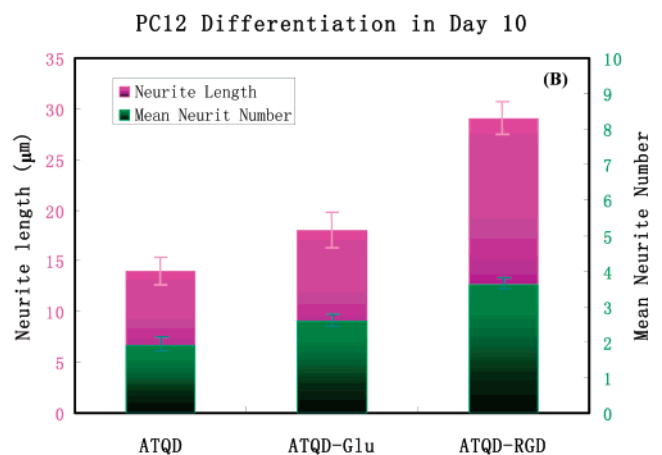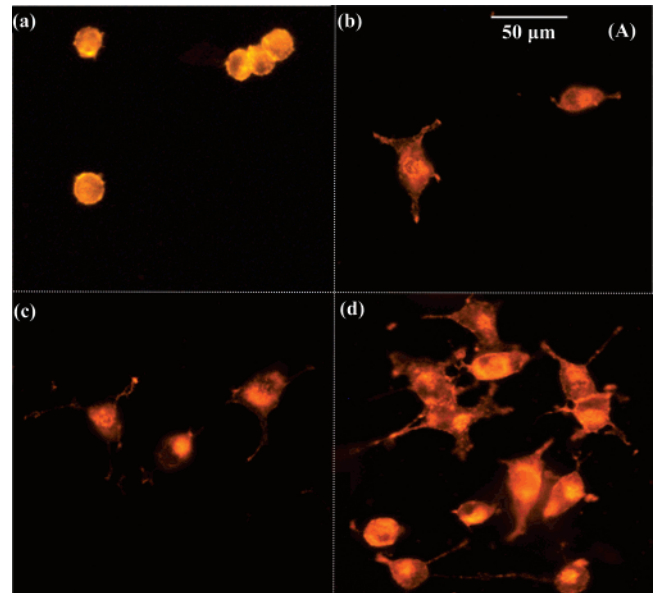

Figure 7. (A) Visualization of PC12 neurite outgrowth by fluorescence micrographs for the substrates (a) glass, (b) ATQD, (c) ATQD−Glu, and (d) ATQD−RGD on day 10. (B) The trend of neurite outgrowth in terms of the mean neurite length and the mean neurite number per cell on day 10. Data are expressed as means $\pm$ SD, $n = 3$; images > 20.

sufficient time for PC12 cell adhesion to an RGD−ATQD-modified surface.

3.4. Cell Proliferation for Long-Term Biocompatibility. Proliferation of PC12 cells on ATQD−RGD surfaces was compared to that on four reference substrates: TCP, untreated glass, ATQD, ATQD−glutaraldehyde (ATQD−Glu). All data were normalized to the AB fluorescence reading at day 1, and the optimal seeding density was determined to be 50 000 cells/well. As seen from the normalized data (Figure 6), attaching the RGD motif significantly improved cell adhesion to and proliferation on the electroactive ATQD−RGD surface. Population doubling times of PC12 growing on the "gold standard" TCP (PD = 2.20 $\pm$ 0.15 days) and the RGD-modified ATQD (PD = 2.30 $\pm$ 0.12 days) were essentially identical (p > 0.88). Cell proliferation on ATQD and ATQD−Glu (p < 0.01) was significantly slower (PD = 2.83 $\pm$ 0.15 days and PD = 3.37 $\pm$ 0.22 days, respectively), probably because of the poor cell adhesion to these substrates. This finding confirms our previous results that demonstrated moderate biocompatibility of PANi-coated surfaces for PC12 cells, which was significantly enhanced by grafting (through a chloromethylation approach) adhesive peptides.[9] On the other hand, the biocompatibility of PANi may be cell-type dependent, since, for example, H9c2 cardiomyocytes adhered and proliferated well on unmodified doped PANi surfaces.[19] The biocompatibility of ATQD-modified conductive surfaces for other cell types remains to be tested.

3.5. Cell Neuronal Differentiation and Morphology Study. The effects of the surface modifications on the functional differentiation of PC12 cells toward the neuronal phenotype were explored using fluorescence and phase-contrast microscopy. Control glass substrates and TCP substrates were pretreated with glutaraldehyde and RGD solutions for a parallel comparison. The time course of PC12 cell differentiation seeded on the various substrates in the absence or presence of exogenous NGF was assessed for up to 10 days, as detailed in the Experimental Section.

Remarkably, PC12 cells extended their neurites to different degrees on all electroactive substrates, but not on TCP, in the absence of NGF (Figure 7A). When grown on ATQD−RGD-derivatized surfaces, the cells produced longer neurites, which eventually formed the intricate network (Figure 7A(d)). After 6 days, image analysis illustrated a statistically pronounced increase (p < 0.05) in the number of neurites per cell and the mean neurite length (Figure 7B) for each of the electroactive substrates. Throughout the study, the mean length of spontane-
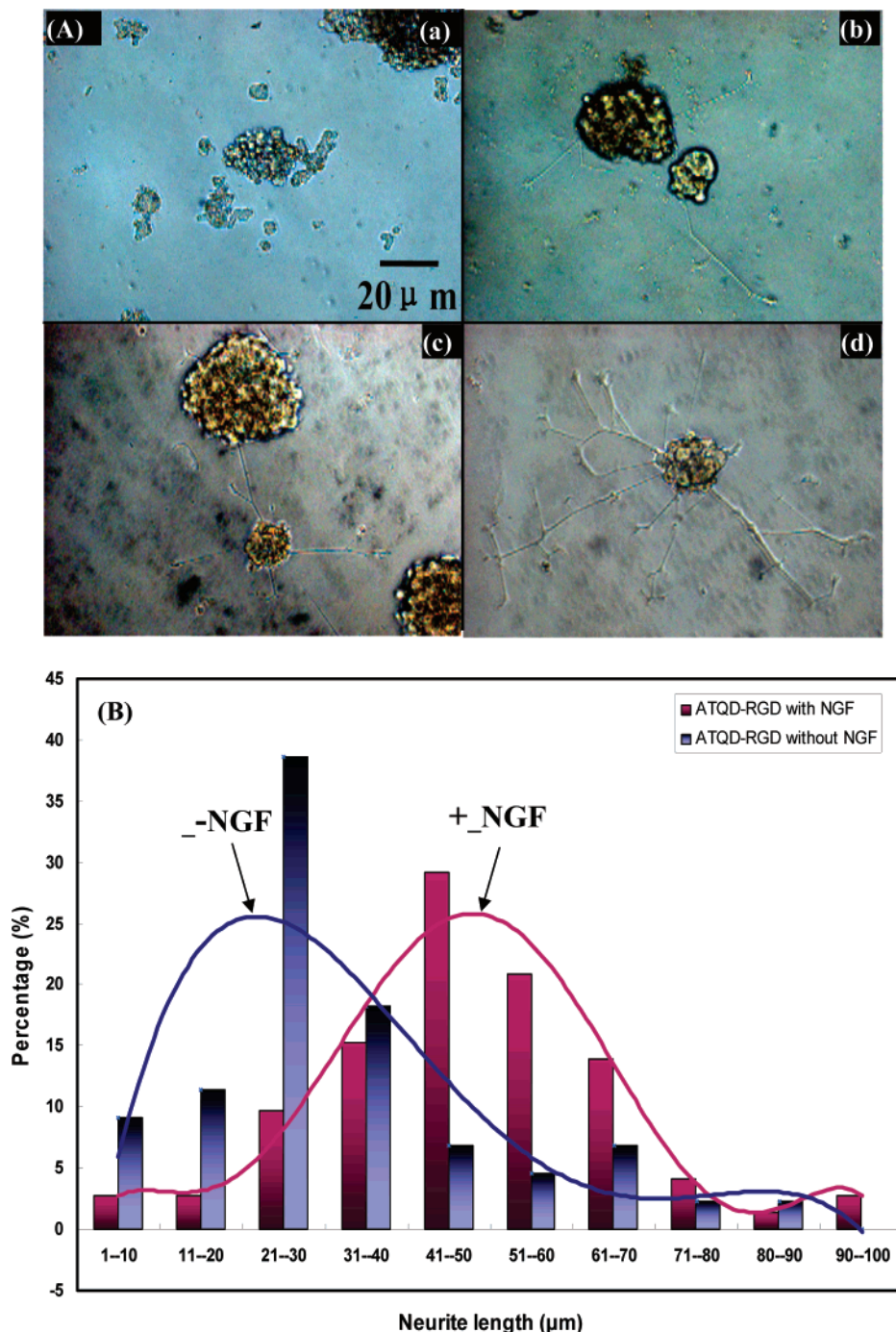
Figure 8. (A) Phase contrast images of PC12 cell morphology for (a) TCP, (b) TCP with NGF, (c) ATQD−RGD, and (d) ATQD−RGD with NGF on day 10 (B) Neurite length distribution chart for ATQD−RGD substrates with and without NGF.

ous PC12 neurite extension in the absence of NGF increased steadily over the duration of the experiment, with ATQD−RGD being the most neuritogenic surface. On day 10, the neurites of cells cultured on ATQD−RGD were extended by 3.6 ± 0.3 μm on average, resulting in a mean neurite length of 29 ± 2.7 μm (Figure 7A(d)). In contrast, there was no observed neurite extension for cells grown on the unmodified glass substrates (Figure 7A(a)).

As expected, NGF induced significant neurite extension on all surfaces studied (Figure 8A). Analysis of the neurite length showed a pronounced increase in the mean neurite number and neurite length of PC12 cells grown on the ATQD−RGD-modified surfaces compared to the spontaneous neuritogenesis discussed above (Figure 8B). On day 10, nearly 40% of the

PC12 cells grown on the "bare" ATQD−RGD substrates had a neurite length in the range of $21-30$ μm, whereas the addition of NGF essentially doubled the mean length of the neurites (Figure 8B). Instead of extending individual neurites only from the periphery of ganglion-like PC12 clumps, NGF induced the formation of complex, branching neuronal networks and consequently resulted in an increase in the mean neurite number from 3.4 ± 0.5 to 4.5 ± 0.6. As compared to the control TCP pretreated with RGD under the same conditions, PC12 cells exhibit a remarkable preference for the ATQD-modified surfaces. In line with reports by others (e.g., Fujita et al., 1989),[5] only approximately 35% of our PC12 cells seem to respond to NGF stimulation by extending a few neurites when cultured for 6 days on TCP (Figure S7, Supporting Information). In

contrast, during the same time period, 83% of the cells cultured on ATQD−RGD developed multiple branching axons (Figure 8A).

These data confirm and extend our previous observations, in which we demonstrated that PC12 cells spontaneously extend neurites on conductive PANi surfaces modified with the laminin-derived adhesive peptide YIGSR in the absence of NGF.[9,15] Since the cell-binding motives of RGD and YIGSR by themselves lack neuritogenic activity,[36] we conclude that the electroactivity from the novel substrates may contribute to the cell differentiation as an effective stimulus. These results are also in line with recent observations, in which electroactive surfaces, in the absence of electrical stimulation, enhance the differentiation of embryonic stem cells toward the cardiac phenotype [Bidez, P. R., III. Enhanced cardiac-specific differentiation of mouse embryonic stem cells via electrical stimulation. Ph.D. Thesis, Drexel University, Philadelphia, PA, 2006.] Taken together our results provide evidence that electroactive surfaces may have intrinsic differentiative properties, which may be desirable and useful for engineering excitable tissues, such as neurons and muscle.

4. Conclusion

Novel biomaterials that can structurally mimic an ECM and enhance the interactions with anchorage-dependent cells are highly critical in providing the optimal environment for the appropriate maintenance of cell structure and function in vitro. Therefore, we synthesized a novel electroactive oligoaniline and constructed from it, for the first time, an electroactive heterobifunctional SAM, where one side was covalently bound to the substrate surface and the other was modified with a bioactive RGD motif for improved biocompatibility. This strategy resulted in more direct cell−biomaterial interactions, in which the cells are effectively surrounded by bioactive (RGD) peptide domains and, hence, respond preferentially to the intrinsic proliferative/differentiative cues of electroactive surfaces. Our work demonstrates that our novel electroactive surface can support the adhesion and differentiation of PC12 cells and, remarkably, that the intrinsic electroactive properties of the surface-enhanced neuritogenesis in the absence of neurotrophins. The novel electroactive SAMs from ATQD can provide a platform for anchoring bioactive molecules or specific functional moieties for electrocatalytic application,[37] biosensors,[38] and optoelectronic devices[39] as well as for cardiac and neuronal tissue engineering.[18−20] Future work will focus on investigating the mechanisms for the spontaneous neuritogenic effects of the electroactive surfaces, extend these studies to generating electroactive three-dimensional scaffolds, and include external electrical stimulation as a means to generate permissive matrices for neuronal bioengineering.

Supporting Information Available. Separation of as-synthesized sample of ATQD via TLC; ^1H NMR, ^{13}C NMR, and high-resolution MS spectra of ATQD; increment of attached calls on ATQD−RGD via AB assay; PC12 cell proliferation on various substrates; Phase contrast images of PC12 cell morphology; SEM micrographs of differentiated PC12 cells; IR spectra of ATQD and ATQD−RGD monolayers; cyclic voltammograms of ATQD; and elemental composition of the emeraldine salt of ATQD. This material is available free of charge via the Internet at http://pubs.acs.org.

References and Notes

(1) (a) Hoecker, H. *Macromol. Symp.* **1998**, *130*, 161. (b) Langer, R.; Cima, L. G.; Tamada, J. A.; Wintermantel, E. *Biomaterials* **1990**, *11*, 738. (c) Wen, X.; Zhang, N. In *Introduction to Biomaterials*; World Scientific Publishing: River Edge, NJ, 2006; p 211.

(2) (a) Coombes, A. G. A.; Rizzi, S. C.; Williamson, M.; Barralet, J. E.; Downes, S.; Wallace, W. A. *Biomaterials* **2004**, *25*, 315. (b) Chen, R.; Curran, S. J.; Curran, J. M.; Hunt, J. A. *Biomaterials* **2006**, *27*, 4453. (c) Buttafoco, L.; Kolkman, N. G.; Engbers-Buijtenhuijs, P.; Poot, A. A.; Dijkstra, P. J.; Vermes, I.; Feijen, J. *Biomaterials* **2006**, *27*, 724. (d) Shalaby, S. W.; DuBose, J. A.; Shalaby, M. In *Absorbable and Biodegradable Polymers*; Shalaby, S. W., Burg, K. J. L., Eds.; CRC Press: Boca Raton, FL, 2004; p 77.

(3) Reddi, A. H. *Key Eng. Mater.* **2001**, *459*, 192.

(4) Greene, L. A.; Tischler, A. S. *Proc. Natl. Acad. Sci. U.S.A.* **1976**, *73*, 2424.

(5) Fujita, K.; Lazarovici, P.; Guroff, G. *Environ. Health Perspect.* **1989**, *80*, 127.

(6) (a) MacDiarmid, A. G. *Angew. Chem., Int. Ed.* **2001**, *40*, 2581. (b) Heeger, A. J. *Synth. Met.* **2001**, *125*, 23.

(7) Karyakin, A. A.; Bobrova, O. A.; Lukachova, L. V.; Karyakina, E. E. *Sens. Actuators, B* **1996**, *33*, 34.

(8) (a) Chehimi, M. M.; Azioune, A.; Bousalem, S.; Ben Slimane, A.; Yassar, A. *Surfactant Sci. Ser.* **2003**, *115*, 245. (b) Rivers, T. J.; Hudson, T. W.; Schmidt, C. E. *Adv. Funct. Mater.* **2002**, *12*, 33.

(9) Guterman, E.; Cheng, S.; Palouian, K.; Bidez, P.; Lelkes, P.; Wei, Y. *Polym. Mater. Sci. Eng.* **2002**, *43*, 766.

(10) Collier, J. H.; Camp, J. P.; Hudson, T. W.; Schmidt, C. E. *J. Biomed. Mater. Res.* **2000**, *50*, 574.

(11) Pedrotty, D. M.; Koh, J.; Davis, B. H.; Taylor, D. A.; Wolf, P.; Niklason, L. E. *Am. J. Physiol.* **2005**, *288*, H1620.

(12) Schmidt, C. E.; Shastri, V. R.; Vacanti, J. P.; Langer, R. *Proc. Natl. Acad. Sci. U.S.A.* **1997**, *94*, 8948.

(13) Shastri, V. R.; Rahman, N.; Martin, I.; Langer, R. *Mater. Res. Soc. Symp. Proc.* **1999**, *550*, 215.

(14) (a) Shastri, V. R.; Schmidt, C. E.; Kim, T.-H.; Vacanti, J. P.; Langer, R. *Mater. Res. Soc. Symp. Proc.* **1996**, *414*, 113. (b) Ateh, D. D.; Navsaria, H. A.; Vadgama, P. *J. R. Soc.* **2006**, *3*, 741.

(15) (a) Wang, X.; Gu, X.; Yuan, C.; Chen, S.; Zhang, P.; Zhang, T.; Yao, J.; Chen, F.; Chen, G. *J. Biomed. Mater. Res.* **2004**, *68A*, 411. (b) Zhang, Z.; Roy, R.; Dugre, F. J.; Tessier, D.; Dao, L. H. *J. Biomed. Mater. Res.* **2001**, *57*, 63.

(16) (a) Kamalesh, S.; Tan, P.; Wang, J.; Lee, T.; Kang, E. T.; Wang, C. H. *J. Biomed. Mater. Res.* **2000**, *52*, 467. (b) Wang, C. H.; Dong, Y. Q.; Sengothi, K.; Tan, K. L.; Kang, E. T. *Synth. Met.* **1999**, *102*, 1313. (c) MacDiarmid, A. G.; Epstein, A. *J. Faraday Discuss. Chem. Soc.* **1989**, *88*, 317.

(17) Mattioli-Belmonte, M.; Giavaresi, G.; Biagini, G.; Virgili, L.; Giacomini, M.; Fini, M.; Giantomassi, F.; Natali, D.; Torricelli, P.; Giardino, R. *Int. J. Artif. Organs* **2003**, *26*, 1077.

(18) Wei, Y.; Lelkes, P. I.; MacDiarmid, A. G.; Guterman, E.; Cheng, S.; Palouian, K.; Bidez, P. R. *Electroactive Polymers and Nanostructured Materials for Neural Tissue Engineering in Contemporary Topics in Advanced Polymer Science and Technology*; Zhou, Q.-F., Cheng, S. Z. D., Eds.; Peking University Press: Beijing, China, 2004; pp 430−436.

(19) Bidez, P. R., III; Li, S.; Macdiarmid, A. G.; Venancio, E. C.; Wei, Y.; Lelkes, P. I. *J. Biomater. Sci., Polym. Ed.* **2006**, *17*, 199.

(20) Li, M.; Guo, Y.; Wei, Y.; MacDiarmid, A. G.; Lelkes, P. I. *Biomaterials* **2006**, *27*, 2705.

(21) (a) Wang, Z. Y.; Yang, C.; Gao, J. P.; Lin, J.; Meng, X. S.; Wei, Y.; Li, S. *Macromolecules* **1998**, *31*, 2702. (b) Wei, Y.; Jamasbi, H.; Li, S.; Cheng, S.; Jansen, S. A.; Sein, L. T., Jr. *Polym. Mater. Sci. Eng.* **2000**, *41*, 1778.

(22) Wei, Y.; Yang, C.; Ding, T. *Tetrahedron Lett.* **1996**, *37*, 731.

(23) Ohmi, T. *J. Electrochem. Soc.* **1996**, *143*, 2957.

(24) (a) Cox, J. C.; Longoria, C. C. *Microchem. J.* **1990**, *41*, 41. (b) Tanaka, S.; Mori, M.; Kodama, K.; Hu, W. *J. Liq. Chromatogr. Relat. Technol.* **2000**, *23*, 197.

(25) Selo, I.; Negroni, L.; Creminon, C.; Grassi, J.; Wal, J. M. *J. Immunol. Methods* **1996**, *199*, 127.

(26) Samet, M. M.; Lelkes, P. I. *The Hemodynamic Environment of Endothelium in Vivo and Its Simulation in Vitro in Regulation of Endothelial Cells by Mechanical Forces*; Lelkes, P. I., Ed.; Harwood Academic Press: London, U.K., 1999; pp 1−32.

(27) Nikolaychik, V. V.; Samet, M. M.; Lelkes, P. I. *J. Biomater. Sci., Polym. Ed.* **1996**, *7*, 881.

(28) Li, M.; Mondrinos, M. J.; Gandhi, M. R.; Ko, F. K.; Weiss, A. S.; Lelkes, P. I. *Biomaterials* **2005**, *26*, 5999.

(29) Li, M.; Mondrinos, M. J.; Chen, X.; Gandhi, M. R.; Ko, F. K.; Weiss, A. S.; Lelkes, P. I. *J. Biomed. Mater. Res.* **2006**, *79*, 963.

(30) Levasseur, M.; Thompson, P. A.; Harrison, P. J. *J. Phycol.* **1993**, *29*, 587.

(31) Huang, L.; Hu, J.; Zhuang, X.; Ma, J.; Chen, X.; Jing, X.; Guo, Y.; Li, M.; Lelkes, P. I.; Wei, Y. *Gaodeng Xuexiao Huaxue Xuebao* **2005**, *26*, 1771.

(32) Kantlehner, M.; Schaffner, P.; Finsinger, D.; Meyer, J.; Jonczyk, A.; Diefenbach, B.; Nies, B.; Holzemann, G.; Goodman, S. L.; Kessler, H. *ChemBioChem* **2000**, *1*, 107.

(33) Wan, M. *J. Polym. Sci., Part A: Polym. Chem.* **1992**, *30*, 543.

(34) (a) Focke, W. W.; Wnek, G. E. *J. Electroanal. Chem. Interfacial Electrochem.* **1988**, *256*, 343. (b) Genies, E. M.; Tsintavis, C. *J. Electroanal. Chem. Interfacial Electrochem.* **1985**, *195*, 109.

(35) (a) Richards, F. M.; Knowles, J. R. *J. Mol. Biol.* **1968**, *37*, 231. (b) Olde Damink, L. H. H.; Dijkstra, P. J.; Van Luyn, M. J. A.; Van Wachem, P. B.; Nieuwenhuis, P.; Feijen, J. *J. Mater. Sci. Mater. Med.* **1995**, *6*, 460.

(36) (a) Sweeney, T. M.; Ogle, R. C.; Little, C. D. *J. Cell Sci.* **1990**, *97*, 23. (b) Graf, J.; Ogle, R. C.; Robey, F. A.; Sasaki, M.; Martin, G. R.; Yamada, Y.; Kleinman, H. K. *Biochemistry* **1987**, *26*, 6896.

(37) Shen, L.; Hu, N. *Biomacromolecules* **2005**, *6*, 1475.

(38) Pan, D.; Chen, J.; Nie, L.; Tao, W.; Yao, S. *Electrochim. Acta* **2004**, *49*, 795.

(39) Sun, X.; Liu, Y.; Xu, X.; Yang, C.; Yu, G.; Chen, S.; Zhao, Z.; Qiu, W.; Li, Y.; Zhu, D. *J. Phys. Chem. B* **2005**, *109*, 10786.